Hybrid Material for Protein Sensing Based on Electrosynthesized MIP on a Mannose Terminated Self-Assembled Monolayer

*Decha Dechtrirat, Nenad Gajovic-Eichelmann, Frank F. Bier, and Frieder W. Scheller**

A novel strategy to prepare a surface confined molecularly imprinted polymer (MIP) film directly on a transducer surface for protein sensing is achieved by combining interaction with a natural binding receptor and binding to a fully synthetic MIP. A thiolated oligoethyleneglycol (OEG)/mannose conjugate is first self-assembled on the transducer surface. Then the carbohydrate binding protein, concanavalin A (ConA), is "vectorially" immobilized as a submonolayer on the underlying mannose modified surface. Afterwards, an ultrathin polyscopoletin film with the thickness comparable to that of the protein is electrodeposited on the top. This architecture ensures that the target is confined to the film surface. The resulting functional material shows an approximately 20-fold higher affinity than that obtained from the mannose self-assembled monolayer. This result shows a synergism between multivalent binding of the natural sugar ligand and the non-covalent interactions of the target within the MIP cavities. Recognition capability of the film is characterized by a real-time measurement using quartz crystal microbalance. In comparison to the non-imprinted film, the imprinted film reveals 8.6 times higher binding capacity towards ConA. High discrimination towards the target protein's homologues shows size and shape specificity of the imprint.

1. Introduction

Molecular recognition plays a key role in most biological processes such as ligand/receptor binding, substrate/enzyme reactions, as well as translation and transcription of the genetic code and is one of the most important talents of nature to selectively distinguish one molecule from another. Nature has created molecular recognition elements mainly based on amino acids and nucleotides as biopolymers typically with high affinity and selectivity against their molecular targets. Therefore, they have been exploited in a wide range of diagnostics and bioanalysis. As an alternative to evolution by the natural selection process, fully synthetic molecularly imprinted polymers (MIPs) have broken new ground by the groups of Wulff, Shea, and Mosbach[1–3] with promising recognition capability, improved stability, reasonable cost, and rapid manufacture.

D. Dechtrirat, N. Gajovic-Eichelmann, Prof. F. F. Bier, Prof. F. W. Scheller
Fraunhofer Institute for Biomedical Engineering
Am Mühlenberg 13, 14476, Golm, Germany
E-mail: fschell@uni-potsdam.de

DOI: 10.1002/adfm.201303148

Molecular imprinting is a strategy to prepare a synthetic molecular recognition unit by polymerizing a functional monomer in the presence of a target molecule as a template. Functionalities on the surface of the molecule to be imprinted initially interact with complementary chemical groups of the surrounding functional monomers in a three dimensional space. The resulting structured orientation has to be conserved by polymerization of the functional monomers yielding to a formation of a size, shape, and functionality specific binding pocket after the template is removed. Over the past few decades, the imprint of small template molecules has been intensively established and a wide range of applications have been explored.[4] Meanwhile, imprinting of macromolecular targets, especially proteins, is also of great interest among researchers. However, protein imprinting is still facing challenges due to their large size with high surface complexity and conformational flexibility.[5–8] To circumvent the problem stemming from the bulkiness of the whole protein, so-called epitope imprinting has been successfully demonstrated where only a selected surface peptide fragment of the protein is templated.[9–14] Another promising strategy to enhance accessibility of the large protein molecule to the imprinted pocket is surface imprinting where the imprinted site is directly generated on the MIP surface. To confine the imprint on the surface, a variety of techniques including microcontact printing with protein stamps,[15–17] and immobilizing protein template on the solid sacrificial supports,[18–21] and preparing an ultrathin film of thickness comparable to the size of proteins[22] have been successfully introduced for the protein binding MIPs.

Most of protein binding MIPs are based on chemical polymerization. Only some of them have used electropolymerization. The advantages of electropolymerization are its abilities to fine-tune the film thickness by controlling the charge consumed during deposition and to grow the film directly at a precise area on the transducer surface. Due to their features, electropolymers have been increasingly used for the preparation of MIP films as sensing elements.[23–25]

Typically for the protein imprint, functional monomers of low molecular weight including acrylic acid derivatives, siloxane derivatives, and electropolymerizable monomers have been

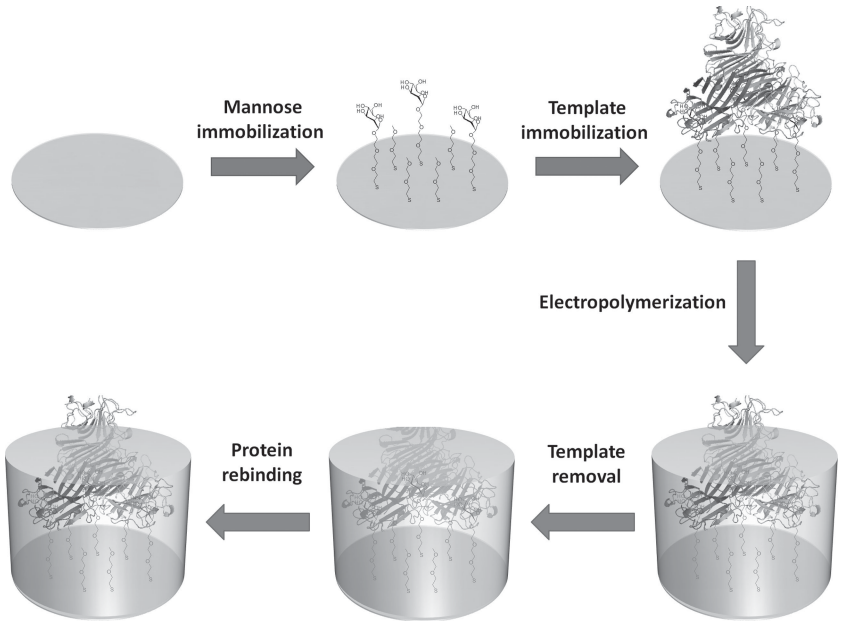

Figure 1. Schematic representation of the template oriented surface imprinting for preparation of hybrid MIP films.

used. Only a few examples have been reported using biomolecules (i.e., lectin,[26] antibody,[26] aptamer[27]) as a high-affinity target-selective building blocks in a hybrid MIP system.

Herein we demonstrate a novel strategy to prepare a hybrid artificial receptor for protein sensing (**Figure** 1) where the self-assembled monolayer (SAM) of the natural binding partner of the target protein and the completely synthetic polymer have been combined in order to enhance the affinity of the resulting functional material. The hybrid can discriminate between the target protein and its homologues resulting from the size and shape specificity of the imprint. Our procedure is straightforward and can be accomplished directly on the transducer surface by only four simple steps: i) a thiolated oligoethyleneglycol (OEG)/sugar conjugate is first immobilized as a mixed SAM with a thiolated OEG spacer on the transducer surface; ii) a sugar binding protein is site specifically immobilized on the sugar modified surface via the sugar/protein interaction as a submonolayer coverage; iii) an ultrathin film with a thickness comparable to that of the protein layer is formed on top of the SAM by electropolymerization allowing the imprint to be confined to the MIP surface; and iv) the protein template is removed by digestion with proteinase K in combination with washing steps leaving the free imprinted sites confined to the film surface.

2. Results and Discussion

To prove the concept, the lectin from *Canavalia ensiformis* (Concanavalin A, ConA), one of the most abundant carbohydrate binding proteins, is selected as a model protein. Since ConA exhibits selectivity for the α-configuration, the mannose probe is designed to possess the α-glycosidic linkage as depicted in **Figure 2**a and will be referred as Mann hereafter. OEG has been broadly reported for its ability to suppress the non-specific adsorption of proteins.[28–30] Therefore, it has been used as a spacer to increase the flexibility of the immobilized ligand and to push the sugar probe away from the surface by a conjugation via a glycosidic bond.[31–33] To raise the affinity of carbohydrate/lectin interactions, nature sums up weak monovalent binding by creating oligomeric forms of lectins. Apart from the geometry of the immobilized mannose probe, the distance between ligands on the 2D flat surface must be presented in a fashion that matches the geometry of the tetrameric structure of ConA in order to attain the enhanced binding affinity via the multivalency effect.

To adjust the density of the ligand, Mann was co-immobilized with a short thiolated OEG linker as binary SAMs at three different molar ratios (1:3, 2:2, and 3:1). Then binding of ConA to the modified SAMs was characterized by using quartz crystal micro-

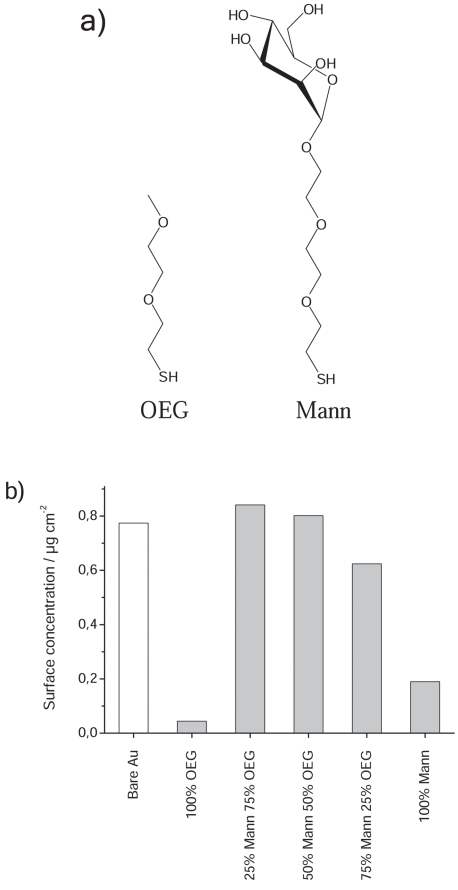

Figure 2. a) Chemical structures of thiolated mannose/OEG conjugate (Mann) and 2-(2-methoxyethoxy)ethanethiol (OEG). b) Adsorbed amounts of ConA at 250 µg mL^{-1} on different surfaces.

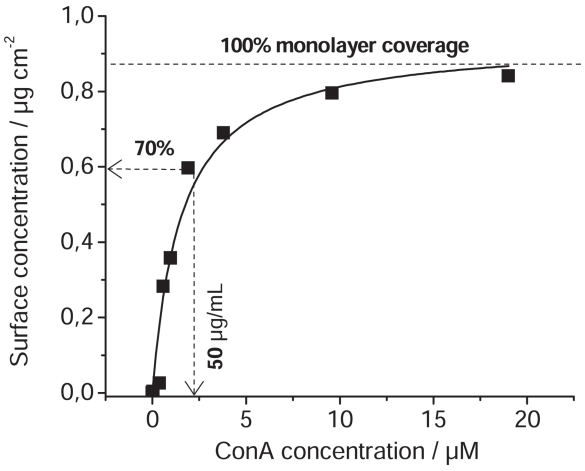

Figure 3. Binding isotherm of ConA to the mannose SAM.

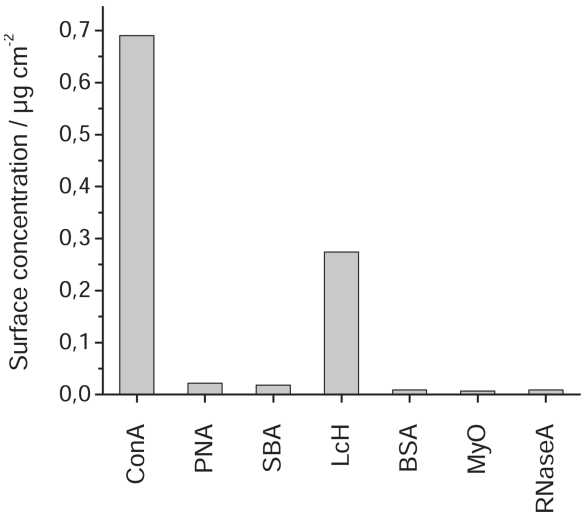

Figure 4. Surface bound amounts of different proteins at 100 µg mL^{-1} on mannose SAM.

balance (QCM) (Figure 2b). Exposing ConA to the bare sensor surface, the observed mass change is clearly due to the non-specific adsorption of ConA to the bare metal electrode. In case of the pure SAM of Mann, the adsorption is assumed to reflect the specific interaction. However, the response is rather low because Mann is too tightly packed so that binding of ConA is hindered. In contrast to the bare gold and pure Mann surface, a pure OEG layer only exhibits a very low response representing the low non-specific adsorption of ConA. When the surface density of Mann is diluted with OEG, the highest response is obtained for the binary SAM prepared by mixing 25% of Mann with 75% of OEG. By increasing the percentage of Mann in the mixed SAM, the response is decreasing as a result of the steric hindrance of the mannose ligand. Due to its highest ConA binding capacity, the Mann/OEG mixed SAM at the molar ratio of 1:3 was used for further experiments.

The adsorption isotherm of ConA on the mannose SAM is constructed by plotting the concentration of protein absorbed on the surface against the protein concentration in solution as depicted in **Figure 3**. The dissociation constant (K_d) of 1.42 µM is determined using the Langmuir adsorption model. The value is in the same range with the previous reports[34–38] on various types of mannose SAM and lower than that obtained from monovalent sugar/protein interaction by two to three orders of magnitude representing the multivalent binding of ConA to the mannose surface. The adsorption of ConA has reached its saturation at around 0.84 µg cm^{-2} which corresponds to a perfect monolayer coverage as calculated using the Sauerbrey equation and the geometrical surface area of ConA estimated from its crystallographic structure (24.37 nm^2). The template concentration of 50 µg mL^{-1}, which results in a submonolayer coverage of 70%, was chosen to reduce surface protein-protein interactions while maintaining the optimal binding capacity of the resulting MIPs.

Selectivity of the modified mannose SAM against various proteins either related in structure or function as well as non-related controls is illustrated in **Figure 4**. The sensorgrams are shown in Figure S1 (Supporting Information). For the control proteins which are not-related to ConA neither in function nor structure (i.e. BSA, Myo, and RnaseA), the observed responses are nearly negligible. These could be explained by their lack of mannose binding sites and the excellent ability of OEG to suppress the non-specific adsorption. The tetrameric lectin homologues from peanut and soybean (i.e., PNA and SBA) which express a high degree of primary sequence identity and tertiary structure similarity to ConA are selected as the control proteins. Even though the structures of these two lectins are similar to ConA, their sugar specificities are galactose instead of mannose. Due to their dissimilarity in sugar binding which is derived from a natural evolution process called circular permutation, PNA and SBA show only small adsorption to the mannose SAM. An interesting control protein is the lectin from lentil (LcH) which is known to bind to mannose as well. A relatively high response to the mannose SAM is observed. However, the observed mass change is not as high as ConA because LcH (49 kDa) exists as a dimer with two mannose binding sites and its molecular weight (MW) is only a half of ConA (102 kDa). In addition, the distance between each mannose binding site of LcH (69 Å, PDB entry 1LES[39]) is slightly shorter than that of ConA (74 Å, PDB entry 3CNA[40]) which may possibly affect the binding of LcH to the immobilized mannose. Although the mannose SAM has been proven to be highly inert against most of the control proteins, binding of mannose binding proteins is obvious. We therefore aim to increase the selectivity of our system against this class of proteins by integrating our mannose SAM with a MIP layer.

A scopoletin based non-conductive electropolymer which has been pioneered by our group[41] is used[14,42] as a MIP matrix. A superior feature of this electropolymer is its low oxidation potential range (0.4–0.7 V vs Ag/AgCl). Under such conditions, the oxidative desorption of the thiol group is negligible, making it possible to deposit the film on top of the SAM.[14] In comparison to bulk protein imprinting, our strategy with the pre-immobilization of protein template on the solid surface offers an improvement of imprinting efficiency by reducing the conformational space and the thermodynamic motion of the template in solution.[43] Moreover, a uniform template orientation

Table 1. Dependence of percentage of template removal on monomer concentration, and the film thickness.

Monomer concentration [mM]	Film thickness[a)] [nm]	Template removal [%]
0	–	≈99
0.25	≈3.4	≈92
0.50	≈6.3	≈89
1.00	≈7.7	≈40

[a)]Estimated by surface plasmons spectroscopy (SPS).

is obtained by site-specific immobilization of ConA to the mannose surface via its sugar binding pocket. To fine-tune the film thickness on a nanometer scale, the potential pulse method was employed. By applying a pulse at potential of 0.7 V for 5 s while varying the concentrations of the monomer, ultrathin films with different thicknesses were obtained. Proteinase K was used to digest the surface confined protein template. In combination with a washing step, the protein fragments were successfully removed leaving the free imprinted sites behind. Decrease in fluorescence intensity after the removal of TAMRA labeled ConA was used to calculate the percentage of template removal. The template removal efficiency at different film thicknesses is summarized in **Table 1**. In the absence of the polymeric film, the immobilized protein was completely removed. According to the experimental result obtained by surface plasmons spectroscopy (SPS), the thickness of the protein layer immobilized on the mannose SAM is ≈6.8 nm which is in good agreement with the value of protein reported in the literature (≈6.7 nm)[44] and also the value estimated from the crystallographic structure (≈7.0 nm). The film of thickness of ≈3.4 nm, which is roughly a half of the protein size, is obtained by electrodepostition of scopoletin with the concentration of 0.25 mM. Since only a half of the protein is embedded within the polymeric matrix, the template removal efficiency is still as high as without the film. As the film thickness nearly reaches the size of the protein, roughly 89% of the template could be efficiently removed. For films with higher thickness than the protein size, the percentage of the template removal is significantly reduced down to 40% due to the entrapment of the protein within film matrix. The resulting number is remarkably high as compared to the conventional bulk imprinting technique. Therefore, 0.50 mM of scopoletin was chosen as the optimal monomer concentration for the subsequent preparation of the MIP film.

The binding of ConA to the MIP and the control non-imprinted (NIP) films was monitored in real time by QCM measurements. The typical sensorgrams are shown in Figure S2 (Supporting Information). Binding of the protein to the sensor surface will result in a decrease in frequency of a quartz crystal resonator which is directly related to the bound mass of protein by Sauerbrey equation. Following the equation, the amount of bound protein could be calculated. The adsorption isotherms of ConA to the MIP and NIP films are depicted in **Figure 5**. The maximum surface concentration of ConA bound to the MIP film is 0.58 μg cm^{-2} which is approximately 69% of the maximum amount of ConA bound to the mannose

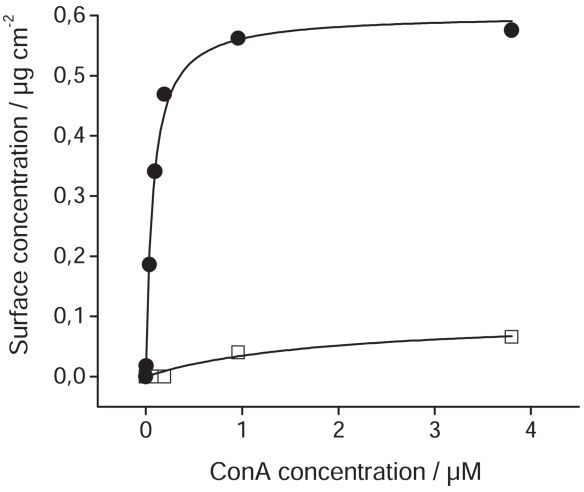

Figure 5. Binding isotherms of ConA to the MIP (solid circles) or NIP film (open squares).

SAM. This value is in accordance with the coverage of 70% of the protein template immobilized on the mannose SAM during electropolymerization. It clearly indicates that at saturation of rebinding all binding sites are occupied by the target protein. In comparison to the NIP film, the imprinted film clearly shows higher binding capacity. At the highest concentration where the binding of ConA has reached its equilibrium, an imprinting factor of 8.6 which is defined as a ratio of the binding capacity of the MIP and the NIP film is attained. The binding of ConA to the control NIP film, which lacks imprinted sites, is attributed to the non-specific adsorption of the protein to the polymer surface. The isotherm of the MIP film is fitted with the Langmuir adsorption model yielding to the dissociation constant (K_d) of 72 nM. This indicates a relatively strong interaction between the target protein and our imprinted film. As compared to the plain mannose SAM, the binding affinity of our hybrid MIP film has been improved by the factor of 20 due to a synergistic effect between the underlying mannose SAM and the covering MIP layer.

Cross reactivity of the imprinted film was determined for non-related proteins (i.e., BSA, Myo, RNaseA) and other lectins (i.e., PNA, SBA, LcH) as depicted in **Figure 6**. The sensorgrams are shown in Figure S3. The adsorption of each protein has reached steady state after ≈10 min due to the high accessibility to the mannose SAM and the surface-confined imprinted site in case of ConA. The binding of ConA to the mannose SAM shows considerably fast dissociation after the injection of protein-free buffer as compared with the MIP surface. The binding of BSA, Myo, and RNaseA to the MIP and the NIP film shows no preference to either of the two films indicating that this binding is derived from the non-specific adsorption. As the pI values of BSA (4.6–4.9), Myo (6.8–7.2), and RNaseA (9.3–9.6) are different, they are negatively charged, neutral, and positively charged, respectively at the physiological pH of the binding buffer. Since they are comparably bound, the non-specific adsorption is not dominated by electrostatic but rather by hydrophobic interactions. In spite of the similar primary, secondary, and tertiary structures of PNA and SBA, their

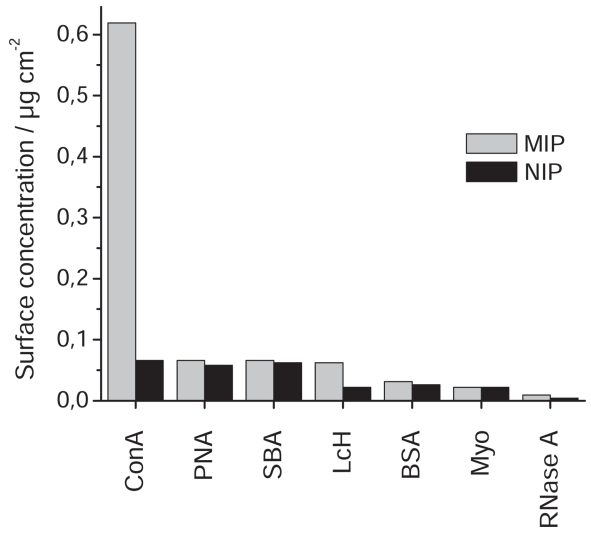

Figure 6. Surface bound amounts of different proteins at 100 µg mL^{-1} to MIP and NIP film.

quaternary structures are considerably different by the differed association and orientation of the monomer in the dimeric and tetrameric assemblage.[45,46] As a result, PNA and SBA do not fit into the binding site templated by ConA. The observed relatively low protein amounts bound to the MIP are mainly derived from the non-specific adsorption. This confirms that polyscopoletin itself shows low non-specific binding not only to ConA but also to other proteins. In contrast to ConA, LcH exists only as a dimer. As compared to ConA, the primary structure of LcH shows an unusual circular permutation. While each unit of ConA consists of one continuous 237-residue chain, each monomer of LcH is composed of two separated chains (one light α chain and one heavy β chain).[47] Considering the assembly of the monomer in the dimeric structures of ConA and LcH, the variation of their quaternary structures derives from the deviations of angles twisted between each subunit.[45] With its size (49 kDa) roughly a half of ConA (102 kDa), LcH is able to access the cavities generated by ConA. However, the structure of LcH is different from ConA and does not fit into the imprinted pocket. Therefore, the slightly higher binding of LcH to the MIP film as compared to the NIP film is not a result of the imprinting effect but rather caused by the binding of LcH to the mannose. Nevertheless, the binding of LcH to the imprinted surface is not as high as observed on the mannose SAM because of the shape effect of the imprint. This observation has proven that the selectivity of the mannose SAM was enhanced by the imprinting process.

3. Conclusion

We have demonstrated a new strategy to prepare a hybrid MIP for protein sensing, where a natural receptor has been combined with a fully synthetic polymer. The resulting hybrid imprint exhibits an affinity in the same range as antibodies, which is roughly twenty times higher in comparison to the natural ligand. The amplification of the binding is mainly due to a synergism between the multivalent binding to the natural ligand and the collective non-covalent interactions of domains on the target protein and the MIP. The binding capacity of the hybrid imprinted film is ca. 8.6 times higher than that of the control non-imprinted film. Selectivity against the target protein's analogues is obtained by the size and shape exclusion effect of the imprint. Our strategy offers straightforward fabrication of the recognition element on the transducer surface involving electrochemical, acoustic, and optical sensors. In comparison to the microcontact printing approach, there is no need to peel off the MIP film from the stamping substrate which may cause damage of the imprinted site by the applied shearing force. With the electropolymerization protocol, a fine-tuned film thickness is obtained, making it possible to confine the imprinted site on the film surface ensuring high accessibility of the target protein. Using a natural ligand to orient the template during the MIP formation, uniform high affinity binding cavities are generated. Moreover, our approach is versatile and by no means limited to carbohydrate binding proteins. Other small ligands including peptides, protein inhibitors, drugs, or antigens can also be used to direct the immobilization and to enhance the binding affinity.

4. Experimental Section

Materials: Gold coated disks with 200 nm gold layer thickness, gold coated SPR sensor disks, and 10 MHz AT-cut gold coated QCM sensor chips were purchased from Ssens (Netherlands), XanTec bioanalytics GmbH (Germany), and 3T Analytik (Germany), respectively. Scopoletin, concanavalin A (ConA, MW ≈ 102 kDa, pI ≈ 4.5–5.5) from *Canavalia ensiformis*, peanut lectin (PNA, MW ≈ 101 kDa, pI ≈ 5–7) from *Arachis hypogaea*, soybean lectin (SBA, MW ≈ 110 kDa, pI ≈ 6.7–7.0) from *Glycine max*, lentil lectin (LcH, MW ≈ 49 kDa, pI ≈ 8.2–8.8) from *Lens culinaris*, myoglobin (Mb, MW ≈ 17 kDa, pI ≈ 6.8–7.2) from equine heart, ribonuclease A (RNase A, MW ≈ 13.7 kDa, pI ≈ 9.3–9.6) from bovine pancreas, bovine serum albumin (BSA, MW ≈ 66 kDa, pI ≈ 4.6–4.9), Proteinase K from *Tritirachium albumand*, and all other chemicals were purchased from Sigma-Aldrich (Germany) and were of analytical grade or higher. TAMRA labeled ConA was purchased from Invitrogen (Germany). All buffer salts were purchased from Roth (Germany). Ultrapure water from a laboratory water purification system (Sartorius, Germany) was used throughout this work.

Instrumentation: All electrochemical experiments were performed using a Gamry potentiostat Reference 600 (Gamry Instruments, USA). A three-electrode system with a thin-film gold disk, a Pt wire counter electrode, and an Ag/AgCl (1M KCl) reference electrode was used. Fluorescence imaging was performed using a Tecan LS Reloaded microarray scanner (TECAN GmbH, Germany) and the mean fluorescence intensity in arbitrary units for the selected area was calculated automatically by using Array-Pro Analyzer software. To make comparison possible from sample to sample, the scanner settings including scan area, exposure time, and gain were kept constant for all the measurements. Film thickness analysis was conducted with a reflectivity scan surface plasmons spectroscopy mode integrated in a multimode ellipsometer (Multiskop, Optrel GmbH, Germany). More detailed, the sample was placed on the sample holder, aligned perpendicular to the incidence plane of the laser beam (and the reflected laser beam) and illuminated with the 633 nm argon ion laser (1 mW). The reflected beam was detected by a 4-segment photodiode. By varying the incidence angle, the reflection minimum, associated with the surface plasmon resonance, was found. The thickness of the film was calculated from the minimum angle using the known index of refraction

for polyscopoletin (n = 1.455), OEG SAM (n = 1.45),[28] and protein (n = 1.45)[28] with the help of the software included with the instrument. All the real-time, label-free binding experiments were performed using a Gamry eQCM 10M (Gamry Instruments, USA).

Preparation and Optimization of Self-Assembled Monolayers of Thiolated Linker and Thiolated Mannose/OEG Conjugate: Prior to preparation of mannose modified surfaces, gold chip was cleaned using cold oxygen plasma for 10 min. Pure SAMs of Mann and OEG were prepared by immersing the clean gold chip in 2 mM aqueous solution of each thiol. Mixed SAMs of Mann/OEG were obtained by incubating the clean gold chip in binary mixture solution of Mann with OEG at three different mole ratios (1:3, 2:2, and 3:1). The total concentration of thiol in each solution mixture was kept constant at 2 mM. The incubation was performed at room temperature for 3 h in phosphate buffered saline (PBS). After 3 h, the chip was thoroughly rinsed with water, gently dried under N_2 flow, and stored under Ar in the dark until measuring.

Preparation of Surface-Confined Imprinted Film: The clean gold chip was incubated in a binary mixture solution of Mann and OEG2 at a mole ratio of 1:3. The total concentration of thiol in the solution mixture was kept constant at 2 mM. The incubation was conducted in PBS buffer at 25 °C for 3 h. After 3 h, the gold chip was thoroughly rinsed with water, gently dried under N_2 flow. The resulting mannose modified surface was incubated in 50 μg mL^{-1} ConA in 100 mM HEPES buffer of pH 7.4 containing 100 mM NaCl, 1 mM $MnCl_2$, and $CaCl_2$ at 25 °C for 3 h. After 3 h, the chip was thoroughly rinsed with buffer and water, respectively. An aqueous solution of 0.5 mM scopoletin in 100 mM NaCl was freshly prepared and electrodeposition of scopoletin was conducted using a single potential pulse (0.7 V for 5 s, then 0 V for 5 s) without prior deoxygenation of the solution. After electropolymerization, the gold chip was thoroughly rinsed with water. The protein template was removed by treating the film with 100 μg mL^{-1} proteinase K in PBS buffer containing 2% Tween-20 at room temperature for 3 h. Afterwards, the gold chip was gently agitated in PBS buffer for 1 hour to remove the protein fragments, thoroughly rinsed with water, and gently dried under N_2 flow, and stored in the dark until measuring.

Preparation of Non-Imprinted Film: Non-imprinted control film was prepared in an identical manner as those performed in the preparation of the imprinted film, but in the absence of the protein template.

Real-Time Binding Studies using QCM: All binding measurements were performed in 100 mM HEPES buffer of pH 7.4 containing 100 mM NaCl, 1 mM $MnCl_2$, and $CaCl_2$ with a flow rate of 50 μL min^{-1} at 25 °C. For each measurement, the buffer was first injected for 10 min to attain a stable baseline and to reach equilibrium. ConA (over the range of 0.1 to 1000 μg mL^{-1}), PNA (100 μg mL^{-1}), SBA (100 μg mL^{-1}), LcH (100 μg mL^{-1}), Mb (100 μg mL^{-1}), BSA (100 μg mL^{-1}), and RNaseA (100 μg mL^{-1}) were used as the analytes to be investigated. The aqueous solutions of each protein were then injected for a contact time of 10 min at which the steady state has been reached. The protein-free buffer was subsequently injected to remove the unbound protein for 10 min. The report point, at which the binding response was assessed, was recorded at 20 min after the sample loading period. For the concentration dependency experiments, consecutive injections of increasing concentrations of ConA solutions were performed. For the selectivity measurements, the surfaces were regenerated by using 50 mM Glycin/HCl (pH 2.2).

Supporting Information

Supporting Information is available from the Wiley Online Library or from the author.

Acknowledgements

The authors gratefully acknowledge the financial support of BMBF (03IS2201A) of Germany. This research forms part of UniCat, a Cluster of Excellence in the field of catalysis that is coordinated by the Technical University of Berlin and supported financially by the Deutsche Forschungsgemeinschaft (DFG) within the framework of the German Excellence Initiative (EXC 314).

Received: September 10, 2013
Revised: October 28, 2013
Published online: December 9, 2013

[1] G. Wulff, W. Vesper, R. Grobe-Einsler, A. Sarhan, *Macromol. Chem. Phys.* **1977**, *178*, 2799–2816.
[2] K. J. Shea, E. A. Thompson, S. D. Pandey, P. S. Beauchamp, *J. Am. Chem. Soc.* **1980**, *102*, 3149–3155.
[3] R. Arshady, K. Mosbach, *Macromol. Chem. Phys.* **1981**, *182*, 687–692.
[4] C. Alexander, H. S. Andersson, L. I. Andersson, R. J. Ansell, N. Kirsch, I. A. Nicholls, J. O'Mahony, M. J. Whitcombe, *J. Mol. Recognit.* **2006**, *19*, 106–180.
[5] A. Bossi, F. Bonini, A. P. F. Turner, S. A. Piletsky, *Biosens. Bioelectron.* **2007**, *22*, 1131–1137.
[6] T. Takeuchi, T. Hishiya, *Org. Biomol. Chem.* **2008**, *6*, 2459–2467.
[7] Y. Ge, A. P. F. Turner, *Trends Biotechnol.* **2008**, *26*, 218–224.
[8] M. J. Whitcombe, I. Chianella, L. Larcombe, S. A. Piletsky, J. Noble, R. Porter, A. Horgan, *Chem. Soc. Rev.* **2011**, *40*, 1547–1571.
[9] A. Rachkov, N. Minoura, *J. Chromatogr. A* **2000**, *889*, 111–118.
[10] H. Nishino, C. S. Huang, K. J. Shea, *Angew. Chem.* **2006**, *118*, 2452–2456; *Angew. Chem. Int. Ed.* **2006**, *45*, 2392–2396.
[11] D. F. Tai, M. H. Jhang, G. Y. Chen, S. C. Wang, K. H. Lu, Y. D. Lee, H. T. Liu, *Anal. Chem.* **2010**, *82*, 2290–2293.
[12] G. Ertürk, L. Uzun, M. A. Tümer, R. Say, A. Denizli, *Biosens. Bioelectron.* **2011**, *28*, 97–104.
[13] C. H. Lu, Y. Zhang, S. F. Tang, Z. B. Fang, H. H. Yang, X. Chen, G. N. Chen, *Biosens. Bioelectron.* **2012**, *31*, 439–444.
[14] D. Dechtrirat, K. J. Jetzschmann, W. F. M. Stöcklein, F. W. Scheller, N. Gajovic-Eichelmann, *Adv. Funct. Mater.* **2012**, *22*, 5231–5237.
[15] O. Hayden, P. A. Lieberzeit, D. Blaas, F. L. Dickert, *Adv. Funct. Mater.* **2006**, *16*, 1269–1278.
[16] H. Y. Lin, C. Y. Hsu, J. L. Thomas, S. E. Wang, H. C. Chen, T. C. Chou, *Biosens. Bioelectron.* **2006**, *22*, 534–543.
[17] T. Wangchareansak, C. Sangma, K. Choowongkomon, F. L. Dickert, P. A. Lieberzeit, *Anal. Bioanal. Chem.* **2011**, *400*, 2499–2506.
[18] A. Menaker, V. Syritski, J. Reut, A. Öpik, V. Horváth, R. E. Gyurcsányi, *Adv. Mater.* **2009**, *21*, 2271–2275.
[19] G. Lautner, J. Kaev, J. Reut, A. Öpik, J. Rappich, V. Syritski, R. E. Gyurcsányi, *Adv. Funct. Mater.* **2011**, *21*, 591–597.
[20] A. Nematollahzadeh, W. Sun, C. S. A. Aureliano, D. Lütkemeyer, J. Stute, M. J. Abdekhodaie, A. Shojaei, B. Sellergren, *Angew. Chem.* **2011**, *123*, 515–518; *Angew. Chem. Int. Ed.* **2011**, *50*, 495–498.
[21] J. Bognár, J. Szűcs, Z. Dorkó, V. Horváth, R. E. Gyurcsányi, *Adv. Funct. Mater.* **2013**, *23*, 4703–4709.
[22] P. Çakir, A. Cutivet, M. Resmini, B. Tse Sum Bui, K. Haupt, *Adv. Mater.* **2013**, *25*, 1048–1051.
[23] C. Malitesta, E. Mazzotta, R. A. Picca, A. Poma, I. Chianella, S. A. Piletsky, *Anal. Bioanal. Chem.* **2012**, *402*, 1827–1846.
[24] P. S. Sharma, A. Pietrzyk-Le, F. D'Souza, W. Kutner, *Anal. Bioanal. Chem.* **2012**, *402*, 3177–3204.
[25] A. Yarman, F. W. Scheller, *Angew. Chem.* **2013**, *125*, 11735–11739; *Angew. Chem. Int. Ed.* **2013**, *52*, 11521–11525.
[26] T. Miyata, M. Jige, T. Nakaminami, T. Uragami, *Proc. Natl. Acad. Sci.* **2006**, *103*, 1190–1193.
[27] W. Bai, N. A. Gariano, D. A. Spivak, *J. Am. Chem. Soc.* **2013**, *135*, 6977–6984.
[28] K. L. Prime, G. M. Whitesides, *J. Am. Chem. Soc.* **1993**, *115*, 10714–10721.
[29] S. W. Lee, P. E. Laibinis, *Biomaterials* **1998**, *19*, 1669–1675.

[30] T. L. Clare, B. H. Clare, B. M. Nichols, N. L. Abbott, R. J. Hamers, *Langmuir* **2005**, *21*, 6344–6355.
[31] I. H. Min, L. Choi, K. S. Ahn, B. K. Kim, B. Y. Lee, K. S. Kim, H. N. Choi, W. Y. Lee, *Biosens. Bioelectron.* **2010**, *26*, 1326–1331.
[32] F. Tantakitti, J. Burk-Rafel, F. Cheng, R. Egnatchik, T. Owen, M. Hoffman, D. N. Weiss, D. M. Ratner, *Langmuir* **2012**, *28*, 6950–6959.
[33] X. Guo, A. Kulkarni, A. Doepke, H. B. Halsall, S. Iyer, W. R. Heineman, *Anal. Chem.* **2012**, *84*, 241–246.
[34] E. A. Smith, W. D. Thomas, L. L. Kiessling, R. M. Corn, *J. Am. Chem. Soc.* **2003**, *125*, 6140–6148.
[35] P. H. Liang, S. K. Wang, C. H. Wong, *J. Am. Chem. Soc.* **2007**, *129*, 11177–11184.
[36] A. F. Che, X. J. Huang, Z. K. Xu, *Macromol. Biosci.* **2010**, *10*, 955–962.
[37] H. Zheng, X. Du, *J. Phys. Chem. B* **2009**, *113*, 11330–11337.
[38] H. Zheng, X. Du, *Biochim. Biophys. Acta* **2013**, *1828*, 792–800.
[39] F. Casset, T. Hamelryck, R. Loris, J. R. Brisson, C. Tellier, M. H. Daothi, L. Wyns, F. Poortmans, S. Perez, A. Imberty, *J. Biol. Chem.* **1995**, *270*, 25619–25628.
[40] K. D. Hardman, C. F. Ainsworth, *Biochemistry* **1972**, *11*, 4910–4919.
[41] N. Gajovic-Eichelmann, E. Ehrentreich-Förster, F. F. Bier, *Biosens. Bioelectron.* **2003**, *19*, 417–422.
[42] M. Bosserdt, N. Gajovic-Eichelmann, F. W. Scheller, *Anal. Bioanal. Chem.* **2013**, *405*, 6437–6444.
[43] T. Takeuchi, T. Hishiya, *Org. Biomol. Chem.* **2008**, *6*, 2459–2467.
[44] J. Bouckaert, F. Poortmans, L. Wyns, R. Loris, *J. Biol. Chem.* **1996**, *271*, 16144–16150.
[45] M. M. Prabu, K. Saguna, M. Vijayan, *Proteins Struct. Funct. Genet.* **1999**, *35*, 58–69.
[46] V. R. Srinivas, G. B. Reddy, N. Ahmad, C. P. Swaminathan, N. Mitra, A. Surolia, *Biochim. Biophys. Acta* **2001**, *1527*, 102–111.
[47] D. Loganathan, S. E. Osborne, G. D. Glick, I. J. Goldstein, *Arch. Biochem. Biophys.* **1992**, *299*, 268–274.